J. Cent. South Univ. (2014) 21: 2059−2073
DOI: 10.1007/s11771-014-2155-5

Springer

Mechanical behavior and failure analysis of brittle sandstone specimens containing combined flaws under uniaxial compression

YANG Sheng-qi(杨圣奇)[1, 2], JING Hong-wen(靖洪文)[1], XU Tao(徐涛)[3]

1. State Key Laboratory for Geomechanics and Deep Underground Engineering (China University of Mining and Technology), Xuzhou 221008, China;
2. Key Laboratory of Safety for Geotechnical and Structural Engineering of Hubei Province, Wuhan University, Wuhan 430072, China;
3. Center for Rock Instability & Seismicity Research, Northeastern University, Shenyang 110819, China

Abstract: Based on the axial stress−axial strain curves, the effect of fissure angle on the strength and deformation behavior of sandstone specimens containing combined flaws is analyzed. The mechanical parameters of sandstone specimens containing combined flaws are all lower than that of intact specimen, but the reduction extent is distinctly related to the fissure angle. The results of sandstone specimens containing combined flaws are obtained by the acoustic emission, which can be used to monitor the crack initiation and propagation. The ultimate failure mode and crack coalescence behavior are evaluated for brittle sandstone specimens containing combined flaws. Nine different crack types are identified on the basis of their geometry and crack coalescence mechanism (tensile crack, hole collapse, far-field crack and surface spalling) for combined flaws. The photographic monitoring was also adopted for uniaxial compression test in order to confirm the sequence of crack coalescence in brittle sandstone specimens containing combined flaws, which recorded the real-time crack coalescence process during entire deformation. According to the monitored results, the effect of crack coalescence process on the strength and deformation behavior is investigated based on a detailed analysis for brittle sandstone specimens containing combined flaws by using digital photogrammetry.

Key words: brittle sandstone; combined flaws; strength; crack coalescence; acoustic emission (AE)

1 Introduction

Study for mechanical behaviors of rock material containing different pre-existing flaws (such as fissures, holes) has been a significant project in current research. Understanding the strength failure and crack coalescence behavior of rock material is very important to predict unstable failure of engineering rock mass. Although there have been a few experimental investigations on pre-cracked rock to study the crack initiation and coalescence in brittle rock material, most of the works [1−4] have been focused on physical test of model materials (rock-like materials) due to easy fabrication of pre-existing fissures or holes in model specimens, which can be summarized as follows. NEMAT-NASSER and HORII [1] investigated the fracturing mechanisms of flaw plates (model material) and obtained that flaw length is one of the parameters controlling the failure mode of specimen. WONG and CHAU [2] observed three main modes of crack coalescence (tensile, shear and mixed cracks) in flawed model specimens with two fissures in uniaxial compression. PRUDENCIO and VAN SINT JAN [3] presented the results of biaxial tests on physical models of rock with non-persistent joints. Tests showed three basic failure modes: failure through a planar surface, stepped failure, and failure by rotation of new blocks. Planar failure and stepped failure were associated with high strength, and small failure strains, whereas rotational failure was associated with a very low strength, ductile behavior, and large deformation. PARK and BOBET [4] carried out a comparison between experimental observations for gypsum specimens loaded in uniaxial compression, with open and closed fissures, which observed three types of cracks, i.e., wing cracks, coplanar and oblique secondary cracks. Eight types of coalescence were identified, which were applied to specimens with open and closed fissures.

Foundation item: Project(2014CB046905, 2013CB36003) supported by the National Basic Research Program of China; Project(NCET-12-0961) supported by the Program for New Century Excellent Talents in University, China; Projects(51179189, 41272344) supported by the National Natural Science Foundation of China; Project(HBKLCIV201201) supported by the Open Research Fund Program of the Key Laboratory of Safety for Geotechnical and Structural Engineering of Hubei Province, China
Received date: 2012−12−10; **Accepted date:** 2013−05−02
Corresponding author: YANG Sheng-qi, Professor, PhD; Tel: +86−516−83995031; E-mail: yangsqi@cumt.edu.cn

Besides above typical tests on model materials, some real rock specimens have also been tested to investigate the mechanical behaviors of pre-cracked rock materials. FENG et al [5] carried out a number of experimental studies to investigate the mechanism of multi-crack interaction in limestone specimens in size 15 mm (width)×30 mm (height)×3 mm (thickness) with two or three fissures of different arrangements under the coupled uniaxial compressive stress and chemical solutions with different ionic concentrations and pH values. The experimental results indicated that the influence of chemical corrosion was quite complicated, depending on chemical ions and their concentrations and pH values, mineral components of rock, geometry and the number of flaws. WONG and EINSTEIN [6] investigated the cracking behaviors in modeled gypsum and Carrara Marble specimens (76 mm×152 mm×32 mm) containing single open fissure (12.5 mm long and 1.3 mm wide) under uniaxial compression. Seven different crack types were identified based on their geometry and propagation mechanism (tensile/shear) by a high-speed video observation. YANG et al [7] made uniaxial compression tests for cylindrical marble specimens with different pre-existing fissures, which investigated the effect of fissure geometry on strength and deformation failure behaviors. Taking into account triaxial stress state of real engineering rock mass, YANG et al [8] performed conventional triaxial compression tests for cylindrical marble specimens with two pre-existing closed fissures in non-overlapping geometry by fixing the flaw length and ligament length, which investigated the effect of crack coalescence on the axial supporting capacity and deformation behaviors with different confining pressures. The results show that the peak strength and failure mode depend on not only the geometry of flaw, but also the confining pressure.

Sandstone is widely distributed in deep underground engineering, which is a kind of typically sedimentary rock, wherein its strength failure and crack coalescence behavior is very complicated. Therefore, this presented research also becomes more significant. FUJII and ISHIJIMA [9] performed the uniaxial compression tests on sandstone specimens with an inclined slit from the specimen surface or an inclined initial fracture from the specimen surface. The size of the sandstone specimen is 60 mm×120 mm×60 mm, and an inclined slit (open flaw) of 1 mm in thickness and 20 mm in length was introduced. The experimental results showed that the crack from the inclined slit from the specimen surface grew at a small angle to the initial direction and curved slightly towards the free surface in all cases for sandstone specimens. However, no clear relation was observed between the loads at which the main fracture initiated and the inclination of the slit. LU et al [10] carried out the experimental study on cylindrical red sandstone (the size is 50 mm in diameter and 100 mm in length) containing one or two pre-existing fissures under chemical action, which investigated the influence of water chemistry on the mechanical behavior of pre-cracked sandstone. The research results provided understanding of the fundamental nature of rock failure and damage mechanics models for simulating nonlinear evolution of tested red sandstone under coupled mechanical-hydraulic-chemical processes. YANG and JING [11] made uniaxial compression experiments for brittle sandstone specimens (The size of specimen is 60 mm×120 mm×30 mm) containing a single fissure, which investigated the influence of single fissure length and fissure angle on the strength and deformation failure behavior of rock by photographic monitoring and acoustic emission (AE) technique.

Very few experimental works have been reported regarding strength failure and crack coalescence behavior of rock specimens containing combined flaws (combined hole and fissure). LI et al [12] carried out the uniaxial compression experiments on marble (the size is about 110 mm×62 mm×25 mm) with combined flaws, to investigate the propagation and coalescence of cracks in marble specimens. Two types of newborn cracks are observed: wing (tensile) cracks and secondary (shear) cracks. Both types of cracks initiate from the tips of the flaws and propagate in a stable manner. However, he did not get the relation between fissure angle and strength failure parameters, and also did not analyze real-time crack coalescence process and mechanism. As it is well known to us, acoustic emission (AE) technique is an efficient measuring tool to reflect the evolution and propagation of defects in materials, which has been widely applied to investigate the damage and fracture behavior internal the rock material in many past studies [12−15]. In addition, digital photogrammetry is a kind of optical and non-contact measurement technique, which has extensively been used to study the displacement or strain on the surface of a very large range of materials. For example, LI et al [16] investigated the shear patterns and the evolution of local deformation in sands under different confining pressures using digital photogrammetry. SHAH and CHANDRA KISHEN [17] analyzed the mode I and mode II fracture toughness and the critical strain energy release rate for different concrete-concrete jointed interfaces using the digital image correlation technique. LI et al [18−19] presented the application of the close range photogrammetric technique to the model test of tunnel in intermittent jointed rock mass, who found a phenomenon of rock masses re-breaking in broken rock zone. However, up to now, AE and digital photogrammetry techniques were less simultaneously used to explore the initiation,

propagation and coalescence of brittle rock containing combined flaws.

Therefore, in this work, in order to better understand the strength failure and crack coalescence behavior in brittle rock material, uniaxial compression experiments were conducted on brittle sandstone specimens containing combined flaws through the rock mechanics servo-controlled testing system. Moreover, this investigation relied on photographic monitoring and the AE technique to analyze the real-time crack coalescence process during the whole loading. The emphasis of this work is focused on investigating the influence of fissure angle on the strength and deformation failure behaviors of brittle sandstone containing combined flaws, analyzing real-time crack coalescence process in real sandstone material under uniaxial compression on basis of photographic monitoring and the AE technique, and studying the effect of the crack coalescence on the strength and deformation behavior of brittle sandstone specimen using photographic monitoring.

2 Sandstone material and experimental procedure

2.1 Sandstone material

In this work, the sandstone material located in Linyi City, Shandong Province of China was chosen for the experimental object. The sandstone has a crystalline and blocky structure, which is a fine-grained heterogeneous material with average density about 2620 kg/m^3. According to the result of X-ray diffraction (XRD) [11], the minerals in the sandstone specimens are mainly feldspar, quartz, kaolinite and chlorite, and more detailed compositions of this rock are described in Fig. 1.

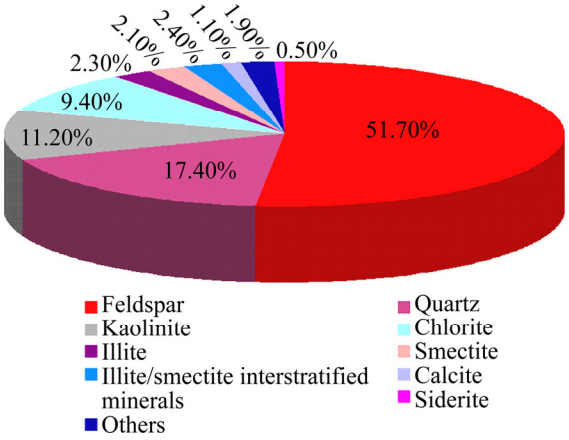

Fig. 1 Composition (mass fraction) of sandstone derived from X-ray diffraction (XRD)

To investigate the mechanical behavior of pre-cracked rock, sandstone specimens containing combined flaws were prepared to perform uniaxial compression tests in natural and dry conditions. The size of all tested sandstone specimens is rectangular with 60 mm in width, 120 mm in height and 30 mm in thickness. The geometry of flawed sandstone is described in Fig. 2. Notice that the term "flaw" is used to describe an artificially created fissure or hole; however, the term "crack" is adopted to describe the new fracture or failure in the process of loading. The geometry of combined flaws is defined by three geometrical parameters—hole diameter d, fissure length $2a$ and $2b$, and fissure angle (the angle of fissure with the direction of the horizontal direction) α as shown in Fig. 2. Notice that the fissures ① and ② are coplanar, and pass through the center of the hole.

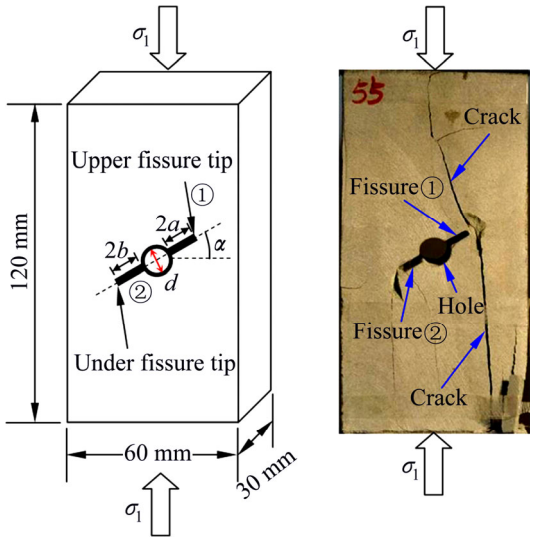

Fig. 2 Geometry of combined flaw in sandstone specimens

In this work, a high pressure water-jet cutting machine was used to cut combined flaws in the intact sandstone specimens [11]. When cutting, the fissure with the length of $2a+2b+d$ = 26 mm was firstly machined in the center of intact specimen, and then the hole were drilled in the center of the specimen containing a single fissure (fissure length equals to 26 mm) in the center. The above machining process can assure that the fissures ① and ② and the center of hole are coplanar. The fissure width was about 2.5 mm. In order to investigate the strength and deformation failure behavior of sandstone containing combined flaws under uniaxial compression, different geometries by varying α while keeping others constant were chosen in the present study. Detailed description for sandstone specimens containing combined flaws is listed in Table 1.

2.2 Experimental procedure

Uniaxial compression experiments on sandstone specimens were carried out in a rock mechanics servo-controlled testing system (MTS815.02) with the maximum loading capacity of 2700 kN and the maximum

Table 1 Sandstone specimens containing combined flaws under uniaxial compression

Specimen	W/mm	H/ mm	T/mm	ρ/(kg·m^{-3})	d/ mm	2a/mm	2b/mm	α/(°)
GS-03#	60.4	120.3	30.0	2625.9	Intact specimen			
GS-52#	60.6	120.3	29.1	2608.0	10	8	8	15
GS-53#	60.4	120.2	29.4	2626.7	10	8	8	15
GS-55#	60.3	120.2	29.6	2596.1	10	8	8	30
GS-47#	60.6	120.2	29.1	2604.0	10	8	8	45
GS-58#	60.5	120.2	29.7	2615.8	10	8	8	60
GS-63#	60.1	119.8	29.5	2642.1	10	8	8	75

Note: W is width; H is height; T is thickness.

displacement capacity of 25 mm [11].

Experimental setup in detail can be described as follows. Firstly, two rigid steel blocks with the size of 63 mm in width, 32 mm in thickness and 15 mm in height were placed between the loading frame and rock specimen. At the same time, two antifriction gaskets were placed between two rigid steel blocks and the end face of rock specimen, which decreased distinctly the effect of the end friction effects on the testing results of sandstone specimens. And then, the axial stress imposed the surface of rock specimen until the failure took place. All the tests were conducted under displacement-controlled conditions with a strain rate of 2.0×10^{-5}. During the uniaxial compression test, in order to investigate the crack coalescence process in the sandstone specimens containing combined flaws subject to stress, the AE technique was adopted. The AE counts were recorded by AE21C-06 acoustic emission system. At the same time, the camera was used to capture images when the coalescence cracks developed or specimen failure occurred. When measuring AE signals, the AE sensors were stuck on the sandstone specimens using vaseline as a coupling agent and fixed slightly by cellulose tape.

3 Strength and deformation behaviors

Figure 3 plots the axial stress−axial strain curve and the failure mode for intact sandstone specimen under uniaxial compression [11], in which the corresponding mechanical parameters are also listed. Here, σ_c is defined as the uniaxial compressive strength and the ε_{1c} refers to peak axial strain. The elastic modulus (E_{av}) refers to the average slope of the more-or-less straight line portion of the axial stress–strain curve, but the deformation modulus (E_{50}) is the slope of the axial stress–axial strain curve at some fixed percentage, generally 50%, of the peak strength. From Fig. 3, it can be seen that the sandstone in this work is very brittle and takes on typically axial splitting failure.

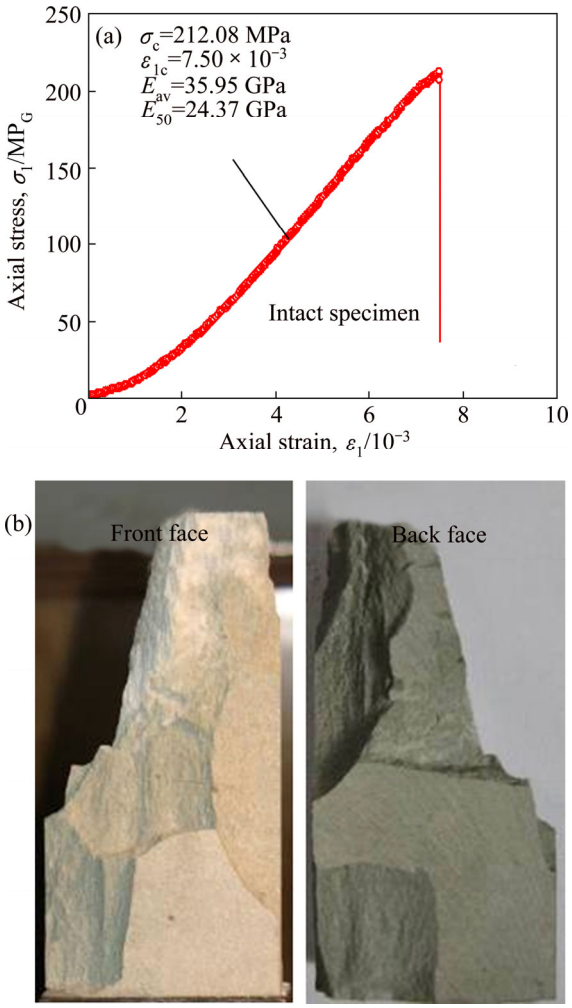

Fig. 3 Axial stress−axial strain curve (a) and failure mode (b) of intact sandstone under uniaxial compression [11]

3.1 Stress−strain curves of brittle sandstone specimens containing combined flaws

Axial stress−axial strain curves of sandstone specimens containing combined flaws (d=10 mm, 2a= 2b=8 mm) with different fissure angles in uniaxial compression are presented in Fig. 4. The corresponding mechanical parameters are listed in Table 2. From Fig. 4 and Table 2, we can conclude that the fissure angle has a

significant effect on the strength and deformation behavior of sandstone specimen containing combined flaws.

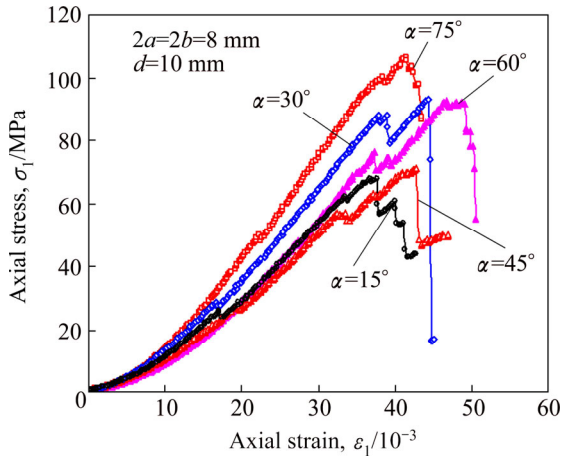

Fig. 4 Axial stress−axial strain curves of sandstone specimens containing combined flaws (d=10 mm, $2a$=$2b$=8 mm) with different fissure angles under uniaxial compression

It needs to be noted that the axial stress−strain curves of sandstone specimen containing combined flaws show several abrupt changes of slope before peak strength, which are coincident with the propagation of some cracks nearby pre-existing flaws along the direction of axial stress [11]. A gradual stress drop after peak strength (e.g., the specimen with fissure angle of 15°) shows the re-fracture mechanical behavior of fractured rock, which results from stable crack coalescence in the specimen. However, a rapid stress drop after peak strength (e.g., thespecimen with fissure angle of 45°) is the result of unstable crack coalescence in the specimen.

3.2 Effect of fissure angle on strength and deformation parameters of sandstone

According to Table 2, the influence of fissure angle on the σ_c, ε_{1c}, E_{av} and E_{50} of sandstone specimen containing combined flaws (Fig. 5) can be summarized. In a word, the mechanical parameters of specimens containing combined flaws are all lower than that of intact specimen, while the reduction extent has a relation with the fissure angle.

The intact specimen has a uniaxial compressive strength of 212.08 MPa, while it could be seen that the uniaxial compressive strength of specimens containing combined flaws ranged from 67.92 MPa (d=10 mm, $2a$=$2b$=8 mm, α=15°) to 106.55 MPa (d=10 mm, $2a$=$2b$=8 mm, α=75°), which the reduction extent of uniaxial compressive strength was between 49.8% and 68.0%. In accordance with Fig. 5(a), it can be seen that the uniaxial compressive strength takes an obvious non-linear relation with fissure angle. But in the previous study [11], the uniaxial compressive strength of brittle sandstone specimen containing a single fissure firstly decreases and then increases with fissure angle. The above two different conclusions result mainly from the difference of crack coalescence process of brittle sandstone containing two different flaw geometries. The uniaxial compressive strength of sandstone specimen containing combined flaws increases firstly from 68.97 MPa (α=15°) to 93.20 MPa (α=30°), and then decreases to 70.85 MPa (α=45°), finally increases to 106.55 MPa (α=75°) from 70.85 MPa (α=45°).

The elastic modulus and deformation modulus of intact specimen were 35.95 GPa and 24.37 GPa, respectively. Compared with that of intact specimen, the decreasing extent of the elastic moduli (Fig. 5(c)−(d)) for sandstone containing combined flaws is dependent to the fissure angle. Take the elastic modulus as an example (Fig. 5(c)). The elastic modulus of specimen containing combined flaws ranged from 24.28 GPa (d=10 mm, $2a$=$2b$=8 mm, α=45°) to 35.42 GPa (d=10 mm, $2a$=$2b$=8 mm, α=75°), and the reduction extent of elastic modulus was between 1.5% and 32.3%. For each specimen, the deformation modulus is usually lower than the elastic modulus, which is due to initial nonlinear deformation at lower loading levels. The elastic moduli have the same trend as uniaxial compressive strength with the increase of the fissure angle, i.e., firstly increase and then decrease, finally increase with increased fissure angle.

The intact sandstone specimen failed at a strain of 0.75% under uniaxial compression, while sandstone

Table 2 Mechanical parameters of sandstone specimens containing combined flaws under uniaxial compression

Specimen	d/mm	$2a$/mm	$2b$/mm	α/(°)	σ_c/MPa	E_{av}/GPa	E_{50}/GPa	$\varepsilon_{1c}/10^{-3}$
GS-03#	Intact specimen				212.08	35.95	24.37	7.500
GS-52#	10	8	8	15	67.92	24.93	15.26	3.761
GS-53#	10	8	8	15	70.02	25.97	16.61	3.966
GS-55#	10	8	8	30	93.20	29.88	19.38	4.448
GS-47#	10	8	8	45	70.85	24.28	14.83	4.281
GS-58#	10	8	8	60	92.89	30.12	17.37	4.671
GS-63#	10	8	8	75	106.55	35.42	22.15	4.145

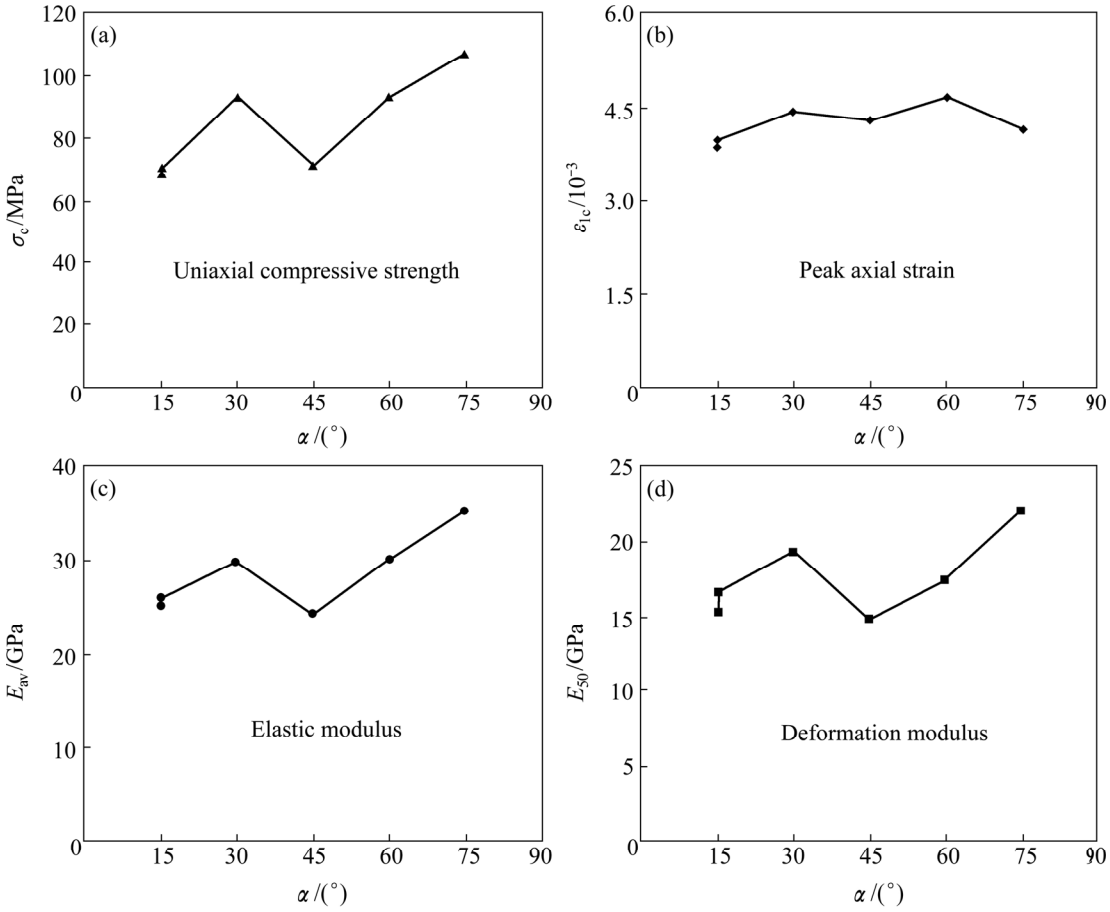

Fig. 5 Effect of fissure angle on strength and deformation parameters of sandstone specimens containing combined flaws (d= 10 mm, $2a$=$2b$=8 mm) under uniaxial compression

specimens containing combined flaws failed at a strain of approximately 0.38%−0.47% (Fig. 5(b)), which were less than that of intact specimen. However, the peak axial strain ε_{1c} of sandstone specimen containing combined flaws is almost not affected by the fissure angle.

3.3 Effect of heterogeneity on strength and deformation behavior

As it is well-known to us, rock is a kind of heterogeneous material. Therefore, we can not obtain completely equal experimental results for two different specimens even though with same testing conditions and specimen scale. Figure 6 shows the effect of heterogeneity on axial stress−axial strain curve of sandstone specimens containing combined flaws (d= 10 mm, $2a$=$2b$=8 mm, α=15°) under uniaxial compression. From Fig. 6, the heterogeneity has nearly no influence on the strength and deformation parameters, and the mechanical parameters of two specimens containing combined flaws (d=10 mm, $2a$= $2b$=8 mm, α=15°) are very approximate. However, the complete axial stress−axial strain curve is dependent distinctly to the heterogeneity. The axial stress−axial strain curve of specimen GS-53# after peak strength is more brittle than that of specimen GS-52#. Moreover before peak strength, the corresponded stress level of two specimens coming out obvious stress drop is different, which results from the effect of the heterogeneity on the crack coalescence process. More detailed analysis will be discussed in the fifth section.

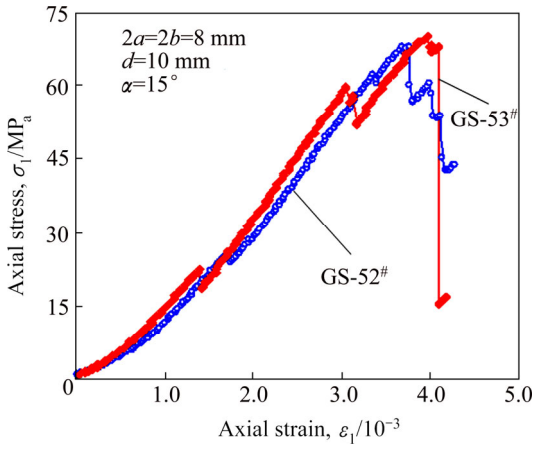

Fig. 6 Effect of heterogeneity on axial stress−axial strain curve of sandstone specimens containing combined flaws (d=10 mm, $2a$=$2b$=8 mm, and α=15°) under uniaxial compression

4 Crack coalescence type and AE behavior

In this section, we will analyze detailed the crack coalescence and AE behaviors of brittle sandstone specimens containing combined flaws under uniaxial compression. For intact specimen, the failure mode is typically axial splitting failure (Fig. 3), which agrees well with many laboratory testing results of brittle rocks. But for sandstone specimens containing combined flaws, we observed different failure modes with that of intact specimen, which are presented in Fig. 7. From Fig. 7, we

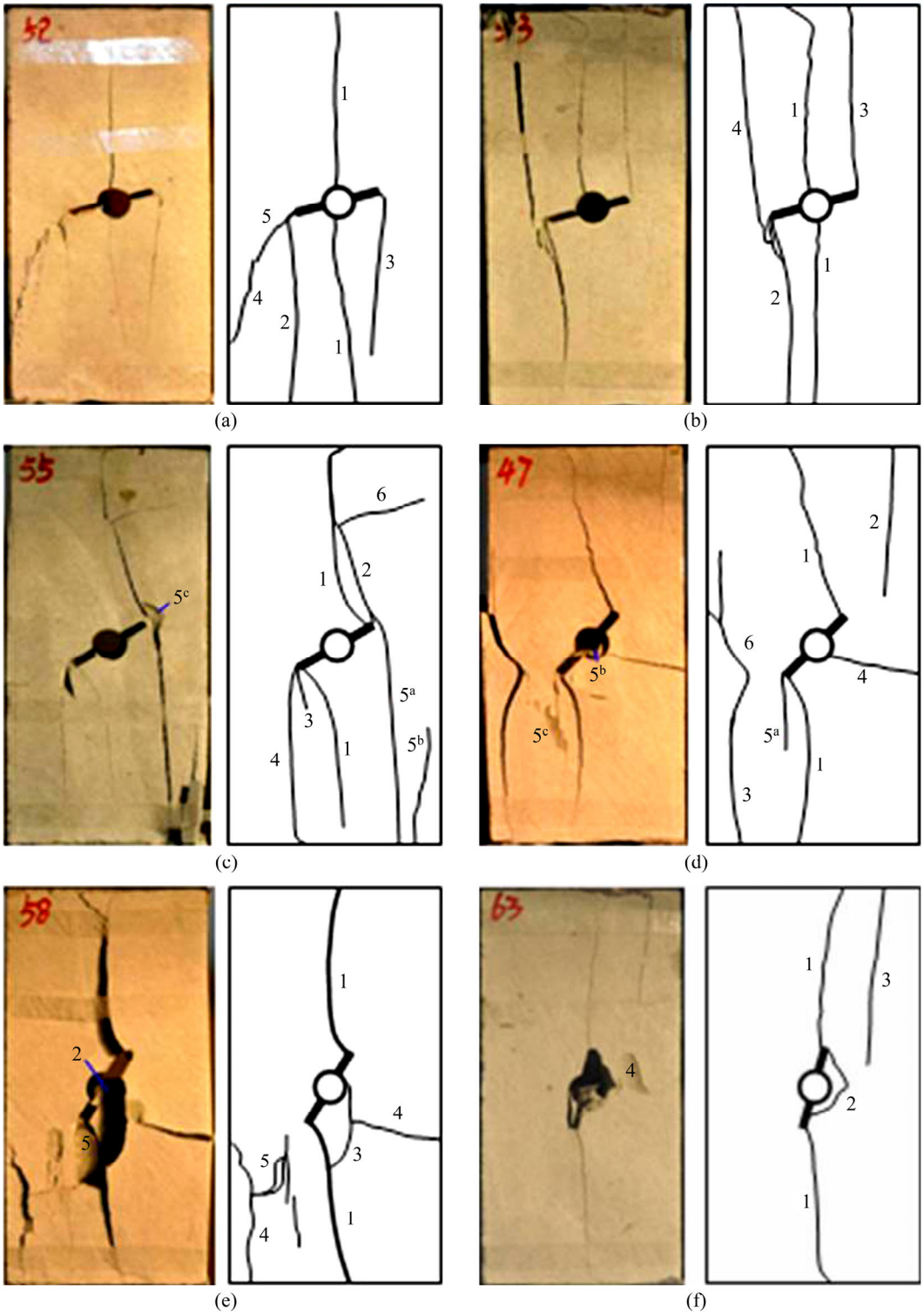

Fig. 7 Ultimate failure modes of brittle sandstone specimens containing combined flaws with different fissure angles (α=15°−75°) under uniaxial compression (d=10 mm, 2a=2b=8 mm): (a) α=15º (GS-52$^{\#}$); (b) α=15º (GS-53$^{\#}$); (c) α=30º; (d) α=45º; (e) α=60º; (f) α=75º

can see that crack coalescences in all the flawed specimens are observed, and depend distinctly on the fissure angle.

4.1 Ultimate failure mode and crack coalescence type

The ultimate failure modes of sandstone specimens showed that nine different crack types (Fig. 8) were identified based on their geometry and crack propagation mechanism (tensile crack, hole collapse, far-field crack and surface spalling) for combined flaws. In accordance with Fig. 8, we can see that six of them (crack types I−VI) are tensile crack, one of them (crack type VII) is hole

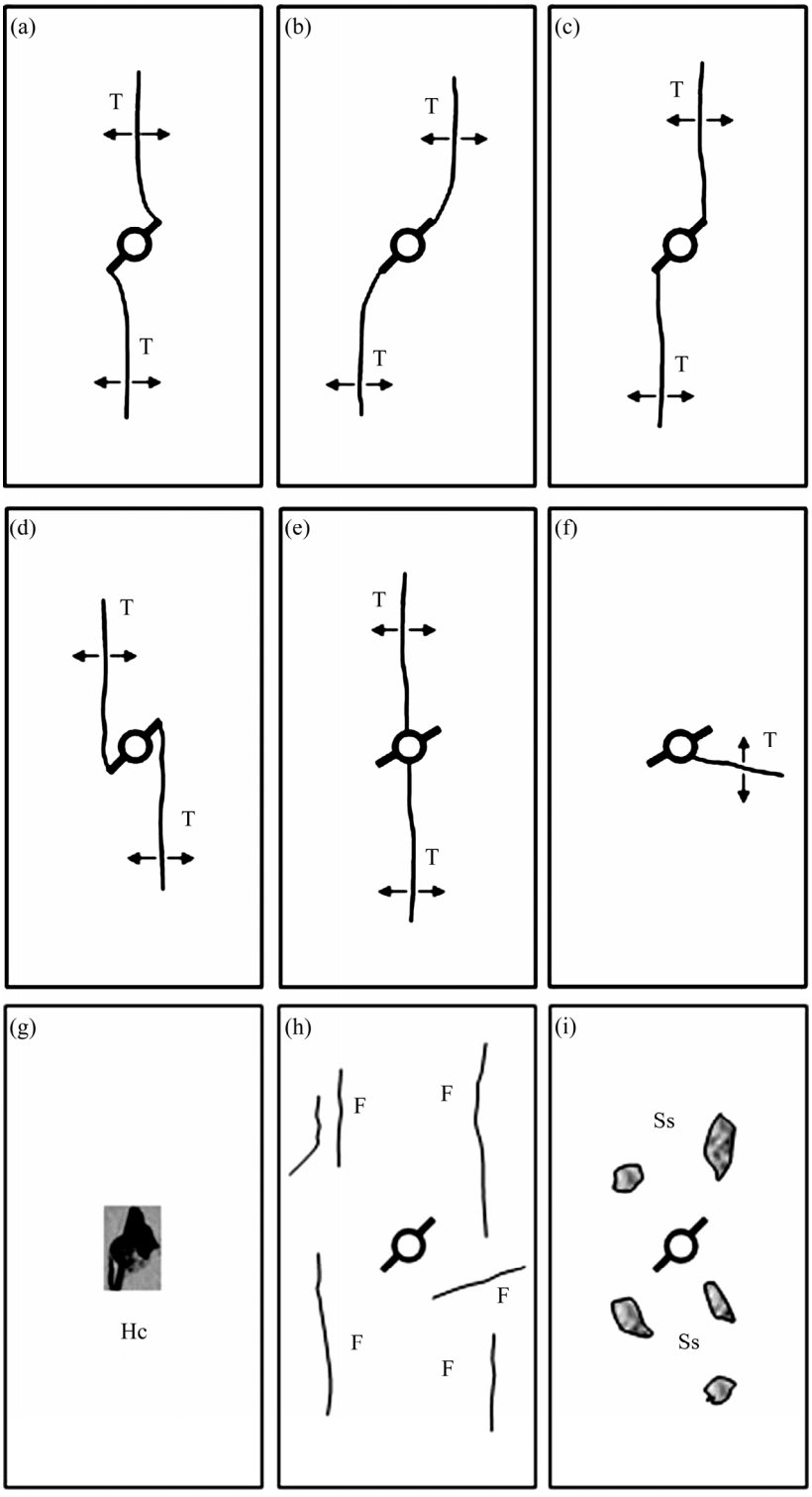

Fig. 8 Various crack types from combined flaws identified in present work. (T for Tensile crack, F for Far-field crack, Ss for Surface spalling, Hc for Hole collapse): (a) Tensile crack (tensile wing crack); (b) Tensile crack (tensile wing crack); (c) Tensile crack; (d) Tensile crack(Anti-tensile crack); (e) Tensile crack(Around the hole); (f) Lateral tensile crack (Around the hole); (g) Hole collapse; (h) Far-field crack; (i) Surface spalling

collapse, one of them (crack type VIII) is far-field crack and one of them (crack type IX) is surface spalling. But it needs to be noted that four of six tensile cracks are initiated from outer tips of pre-existing fissures ① and ②, and two of them are initiated from hole-center.

According to the above nine crack types, the ultimate failure mode and cracking process of sandstone specimens containing combined flaws under uniaxial compression (Fig. 7 and Table 3) can be analyzed. It is very obvious that the macroscopic failure mode of sandstone specimens containing combined flaws (Fig. 7) is a mixture of several cracks among above nine crack types. For example, the failure mode of specimen GS-53# (d=10 mm, 2a=2b=8 mm, α=15°) is a mixture of cracks I and III−V. From Table 3, some qualitative conclusions can be summarized as follows.

Table 3 summarizes initiated crack types of brittle sandstone specimens containing combined flaws with various fissure angles in response to the applied axial loads. As indicated in Table 3, the tensile crack V is the first crack to initiate, and is only observed in two specimens with α=15° (d=10 mm and 2a=2b=8 mm), which shows that this fissure angle makes the specimen containing combined flaws easier to emanate this tensile crack V from hole-center along the direction of axial stress. However, the tensile crack I is usually the first crack initiated from the tips of pre-existing fissures ① and ②, which is often observed for flawed specimens with the fissure angle that is greater than 15°. The anti-tensile crack IV often accompanies with other tensile cracks (e.g., III) towards the reverse direction, while it can be seen that the anti-tensile crack IV is observed in specimen GS-52# without accompanying other tensile cracks. From Table 3, it can be further obtained that the tensile crack III initiates in all the specimens except for specimen GS-58# (α=60°) and tensile cracks II, IV are observed from the fissure tip for the specimens only when the fissure angle is not greater than 30°. Lateral tensile crack VI is very rare, which is only observed in specimen GS-47# (α=45°). Hole collapse VII initiates from the hole-center of pre-existing flaws only when the fissure angle is higher than 45°. Far-field crack VIII is observed in all the specimens except for specimen GS-53# (α=15°). However, surface spalling IX is rarer and easier to occur for brittle rock material, which usually accompanies with other cracks (e.g., cracks III−IV).

4.2 AE behaviors of brittle sandstone specimens containing combined flaws

During the whole loading, the AE behavior of brittle sandstone specimens containing combined flaws under uniaxial compression was recorded simultaneously to further explore the crack coalescence process. Figures 9−12 show the AE counts of brittle sandstone specimens containing combined flaws during compression.

In accordance with Figs. 9−12, we can analyze the influence of fissure angle on the AE behaviors of brittle sandstone specimens containing combined flaws under uniaxial compression. At the stage of fissure closure, the AE events of all the specimens are not active and the AE counts are very rare because little elastic energy was released. Moreover, the AE counts at the stage of fissure closure are not distinctly related to the fissure angle.

With the increase of time, the AE counts come out a larger peak value for all the specimens due to the initiation of the first crack (crack 1) from the tips of pre-existing fissure or hole-center. Afterwards, the elastic deformation will begin to dominate the loading process. At this time, the AE events have still not been active and

Table 3 Initiated crack types of sandstone specimens containing combined flaws under uniaxial compression

Specimen	Crack types								
	I: Tensile	II: Tensile	III: Tensile	IV: Tensile	V: Tensile	VI: Tensile	VII: Hole collapse	VIII: Far-field	IX: Surface spalling
GS-03#	Intact specimen: typically axial splitting failure (Fig. 2)								
GS-52#		√5	√2	√3	√**1**			√4	
GS-53#	√2		√3	√4	√**1**				
GS-55#	√1	√4	√2, 3	√5[a]				√5[b], 6	√5[c] (small)
GS-47#	√1		√5[a]			√4	√5[b]	√2, 3	√5[c] (small)
GS-58#	√1				√3		√2	√4, 5	√5 (more)
GS-63#			√1				√2	√3	√4 (small)

Note: Number represents the precedence relationship of crack coalescence in the specimen. For example, √1 and √2 indicate that the cracks are the first and second cracks to initiate from pre-existing flaws, respectively a, b and c indicate that the cracks are simultaneously initiated in the specimen.

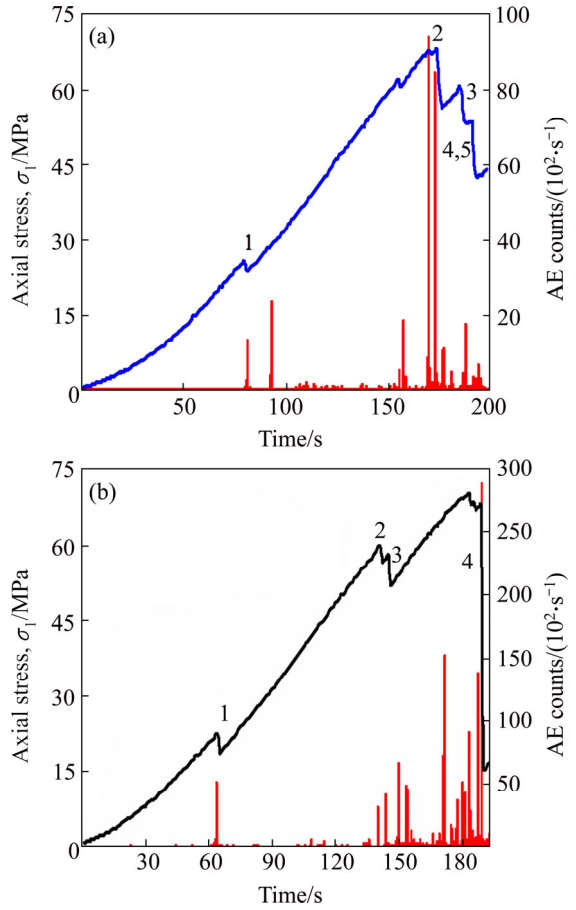

Fig. 9 Relation between axial stress, AE counts and time of sandstone specimen containing combined flaws (d=10 mm, 2a=2b=8 mm, α=15°): (a) Specimen CS-52#; (b) Specimen CS-53#

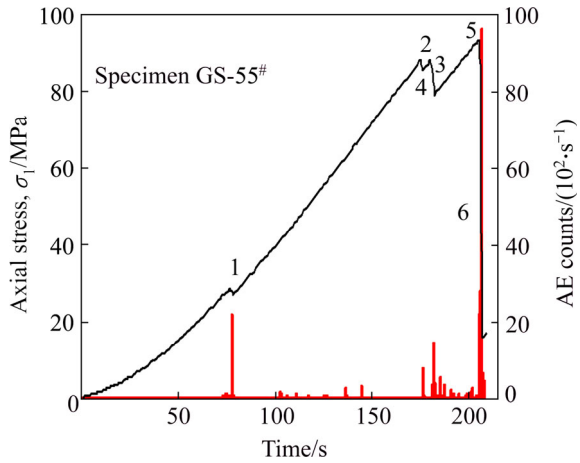

Fig. 10 Relation between axial stress, AE counts and time of sandstone specimen containing combined flaws (d=10 mm, 2a=2b=8 mm, α=30°)

the AE counts are also less, which shows that less elastic energy was released at the stage of elastic deformation. Furthermore, at this stage, no new cracks were observed except for the propagation and widening of the first crack, which will be discussed in detail in the following section.

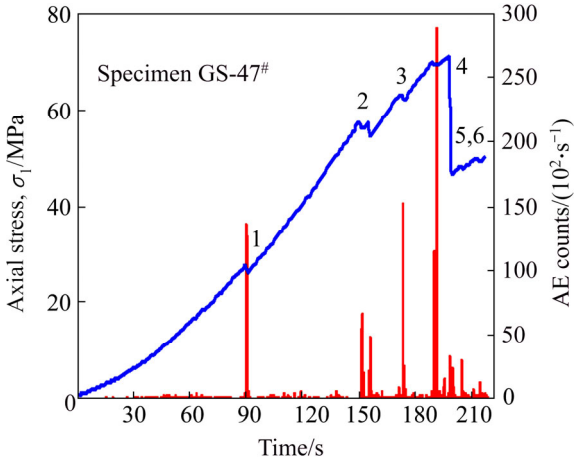

Fig. 11 Relation between axial stress, AE counts and time of sandstone specimen containing combined flaws (d=10 mm, 2a=2b=8 mm, α= 45°)

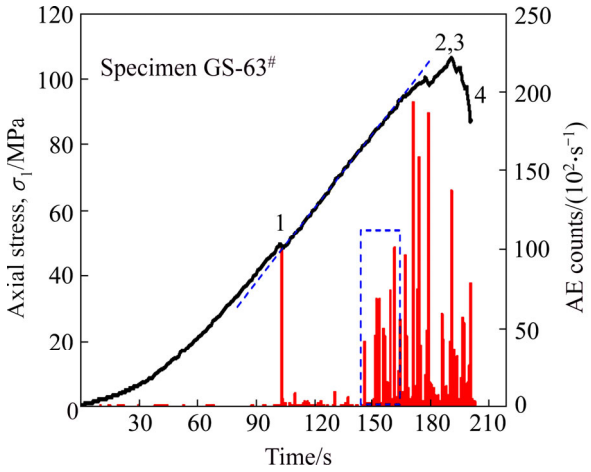

Fig. 12 Relation between axial stress, AE counts and time of sandstone specimen containing combined flaws (d=10 mm, 2a=2b=8 mm, α=75°)

The AE behavior of all other specimens at the stage of elastic deformation were approximately similar except for specimen GS-63# (α=75°) emanating more AE events as shown in rectangle frame of Fig. 12.

After the stage of elastic deformation, the stress−strain curve of the specimen will undergo the stage of crack growth and propagation. With the increase of time, the specimen begins to initiate the second and third larger stress drops in the stress−time curve, which corresponds to higher AE events due to the initiation and propagation of some new cracks. At this stage, the AE events are very active compared with that at the stage of elastic deformation. The AE behaviors at the stage of crack growth and propagation can be predicted approximately the occurrence of rock burst or underground engineering unstable failure (e.g., caving).

When the specimen reaches the strain-softening stage, the axial stress drops rapidly to a very low value.

At this stage, the AE events and counts undergo a relative steady phase. However, we notice that the maximum AE count of some specimens (e.g., GS-52#, GS-63#, etc.) occurs before peak strength in the present research, while the maximum AE count of some specimens (e.g., GS-53# and GS-55#) occurs after peak strength. The above phenomenon implies that the maximum AE count is dependent on not only the fissure angle, but also the heterogeneity of rock material, which can be seen from the comparison between Figs. 9(a) and (b) for two specimens with the same flaw geometry.

5 Real-time crack coalescence process and mechanism

In accordance with previous AE and photographic monitoring results, we can clarify the precedence relationship of crack coalescence in brittle sandstone specimen. Therefore, the real-time crack coalescence process of sandstone containing combined flaws can be analyzed in detail as follows.

Figure 13 presents typical real-time crack coalescence process of sandstone specimens containing combined flaws by using photographic monitoring. From Fig. 13, it is very obvious that the photographic monitoring can be used to identify and characterize the crack coalescence process of brittle sandstone specimens containing combined flaws. Here, the number and letter denoted in Fig. 13 are corresponding to Fig. 9(b) and Table 3. Figure 14 shows typical influence of real-time crack coalescence process on the strength and deformation behavior of brittle sandstone specimens containing combined flaws under uniaxial compression.

From Figs. 13−14, we can analyze real-time crack coalescence process of brittle sandstone specimens containing combined flaws. Before point a (σ_1= 22.40 MPa=14.3% σ_c), the stress concentration nearby combined flaws does not reach the material strength to initiate any cracks. But when the axial stress is loaded to point a, the specimen begins to initiate the crack 1. It needs to be noted that the crack 1 initiates from hole-edge of combined flaws and propagates rapidly to the end parts of the specimen (α=15°), as shown in Fig. 7. The initiation and coalescence of the first crack 1 leads that the axial stress drops to 18.53 MPa from 22.40 MPa in a smaller range of axial strain, which results in a larger AE event as shown in Fig. 9(b). After the first axial stress drop, the axial stress begins to increase

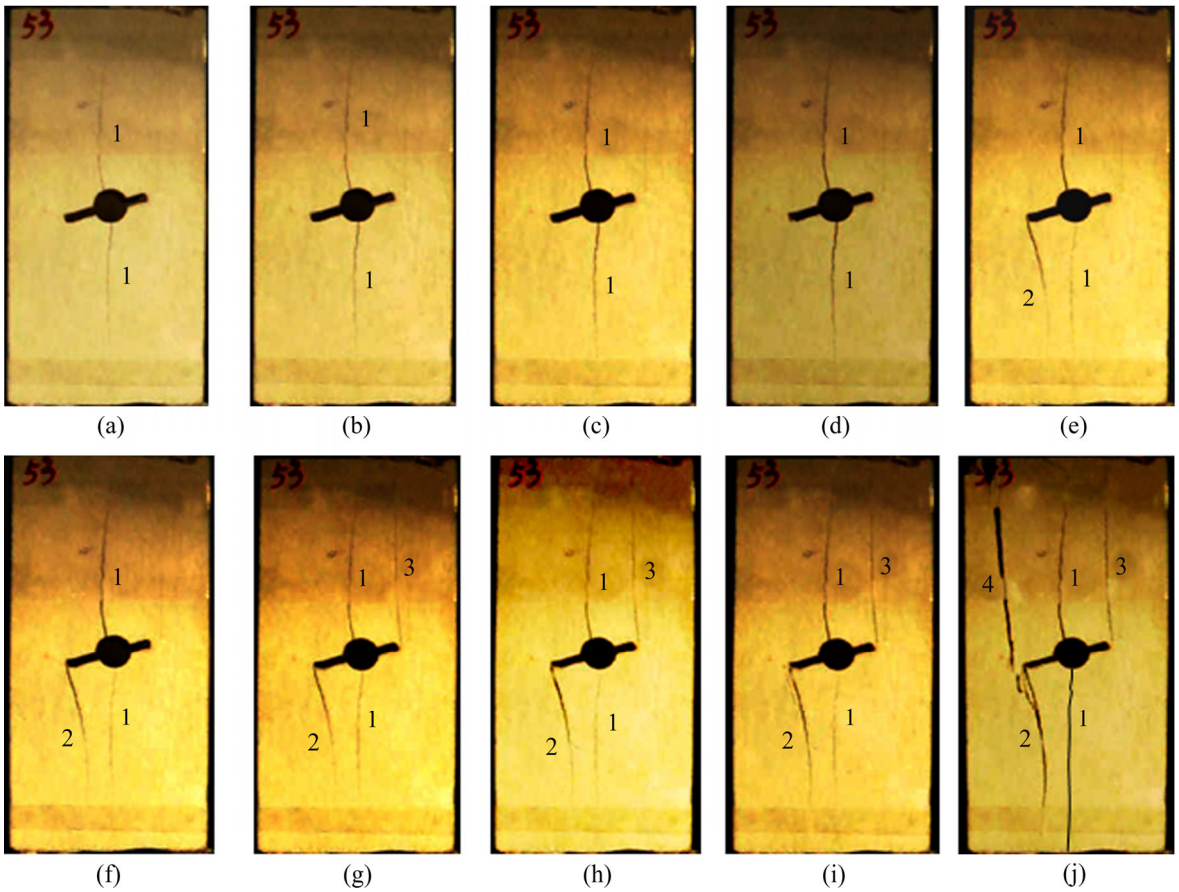

Fig. 13 Typical real-time crack coalescence process of sandstone specimen containing combined flaws (d=10 mm, 2a=2b=8 mm, α=15°) (Denoted number and letter shown in the figure are corresponding to Fig. 9(b)): (a) σ_1=22.40→18.53 MPa; (b) σ_1=30.50 MPa; (c) σ_1=42.07 MPa; (d) σ_1=59.31 MPa; (e) σ_1=59.74→56.45 MPa; (f) σ_1=57.31 MPa; (g) σ_1=58.07→51.94 MPa; (h) σ_1=σ_c= 70.02 MPa; (i) σ_1=67.37 MPa; (j) σ_1=67.89→15.22 MPa

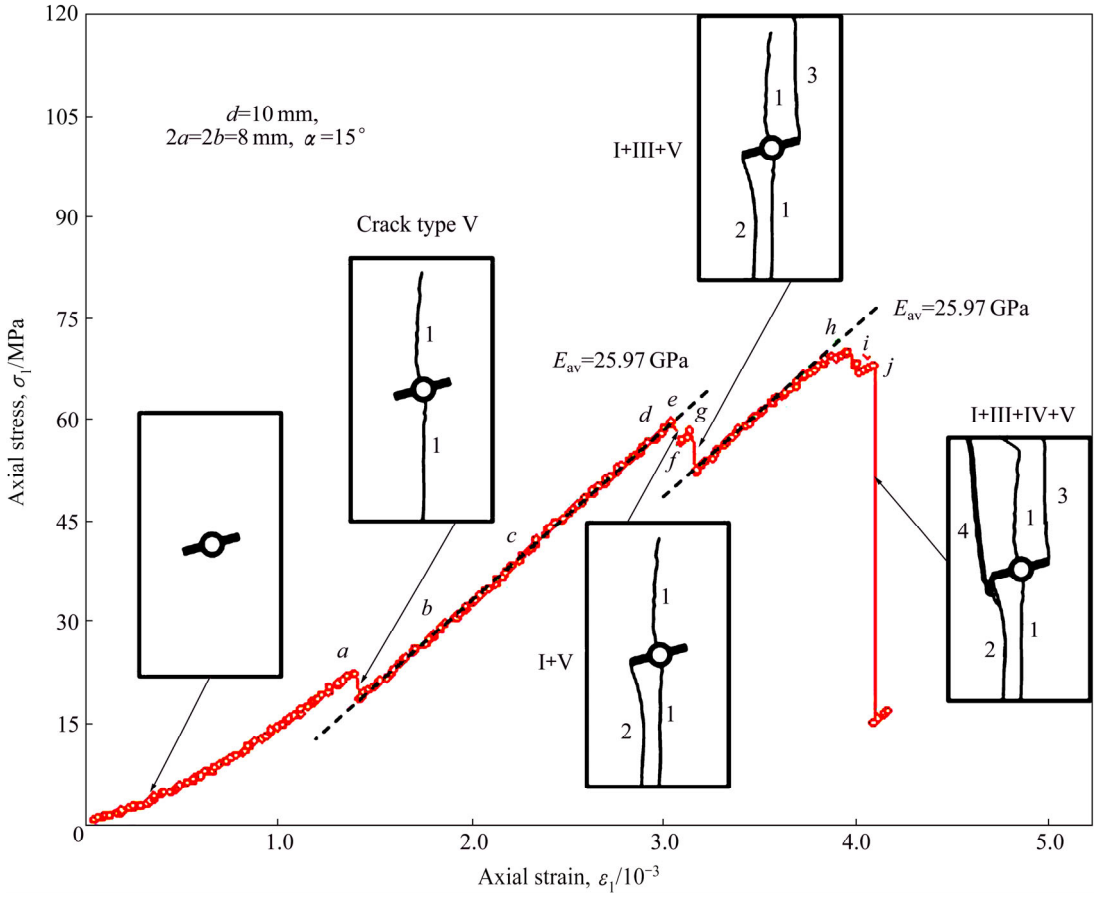

Fig. 14 Effect of real-time crack coalescence on strength and deformation behavior of sandstone specimens containing combined flaws (d=10 mm, 2a=2b=8 mm, α=15°) under uniaxial compression

linearly as the increased axial deformation with the elastic modulus of 25.97 GPa due to a better supporting structure (Fig. 13(a)). The first crack 1 does not lengthen due to the limitation of the specimen boundary but widens and become clearer, which can be concluded from Figs. 13(a)−(d). Therefore, the AE event of this specimen at this stage of elastic deformation is not active. When the specimen is loaded to point e (σ_1=59.74 MPa=85.3% σ_c), the wing crack 2 initiates rapidly from the under tip of fissure ② and propagates to the specimen boundary along the direction of axial stress, which results in the second axial stress drop from 59.74 MPa to 56.45 MPa. Here, it needs to notice that the first crack 1 has a closing tendency when the wing crack 2 produces. Afterwards, with the increase of axial deformation, the specimen undergoes the third axial stress drop from 58.07 MPa to 51.94 MPa, which results from the initiation and coalescence of the wing crack 3 from the upper tip of fissure ① along the direction of axial stress.

After undergoing the second and third axial stress drops, the specimen has still been a good supporting structure (Fig. 13(g)), which leads that the axial stress begins to increase slowly with increased axial deformation. However, it is very obvious that the axial stress−axial strain curve begins to depart the linearity and takes on a typical nonlinear behavior, which results from some internal damages of supporting structure. Rapidly, the continuous increase of axial deformation results in that the specimen is loaded to peak strength (σ_1= 70.02 MPa=100% σ_c). In the loading process, no new cracks are observed from nearby combined flaws but the width of the crack 2 increases and internal damages are more obvious, which will be further analyzed by using digital photogrammetry in the following. Afterwards, the axial supporting capacity of the specimen begins to decrease gradually with the increase of axial deformation. When the axial stress is reduced to point j (σ_1=67.89 MPa=97% σ_c) after peak strength, the tensile crack 4 produces rapidly, which leads to the largest axial stress drops from 67.89 MPa to 15.22 MPa in an almost constant axial strain.

In accordance with the same analysis method as the above specimen, the real-time crack coalescence process of other specimens can also be identified and characterized based on AE results and photographic monitoring. Table 4 lists the subsequence and corresponding axial stress of crack coalescence in brittle

sandstone specimens containing combined flaws under uniaxial compression. In Table 4, the numbers 1−6 represent the subsequence of crack coalescence, as shown in Figs. 9−12. Notice that the axial stress of the initiated first crack 1 from hole-edge is lowest in all the specimens, which shows that the specimen containing this combined flaws (d=10 mm, $2a$=$2b$=8 mm, α=15°) is easier to emanate the tensile crack V, therefore, the peak strength of this specimen is lowest as shown in Fig. 4(a).

From Table 4, we can also further conclude that each larger axial stress drop usually indicates larger crack propagation. For the specimens with bigger fissure angle (e.g., α=60°), the tensile crack I (crack 1) and hole collapse VII (crack 2) do not form at once, but undergo several evolution processes with the increase of axial deformation, which can be concluded from Fig. 15. Here,

Table 4 Sequence of crack coalescence in brittle sandstone specimen containing combined flaws under uniaxial compression

Specimen	Sequence / Corresponding axial stress formed crack in specimen/MPa					
	Crack 1	Crack 2	Crack 3	Crack 4	Crack 5	Crack 6
GS-52#	25.77→23.79	σ_c=67.92→59.91	60.51→58.4	53.65→45.13	45.13→42.77	
GS-53#	22.40→18.53	59.74→56.45	58.07→51.94	67.89→15.22		
GS-55#	28.71→27.23	88.15→85.59	88.07→84.12	84.12→79.23	σ_c=93.20→73.91	73.91→16.27
GS-47#	27.82→26.29	57.11→54.55	62.86→62.17	σ_c=70.85 →48.66	48.66→46.69	48.66→46.69
GS-58#	47.86 ^{k}→46.77, 76.05→70.39	92.04→91.42, 91.61→83.62, 82.62→78.17	92.04→91.42	82.62→78.17	77.91→70.99 →55.12	
GS-63#	49.65→48.13	104.23, σ_c=106.54→105.34→102.51, 101.48→97.29, 97.83→86.81	σ_c=106.54→105.34	97.83→86.81		

Note: The letter k represents the axial stress of initiated the first crack, but the first crack does not propagate the specimen boundary.

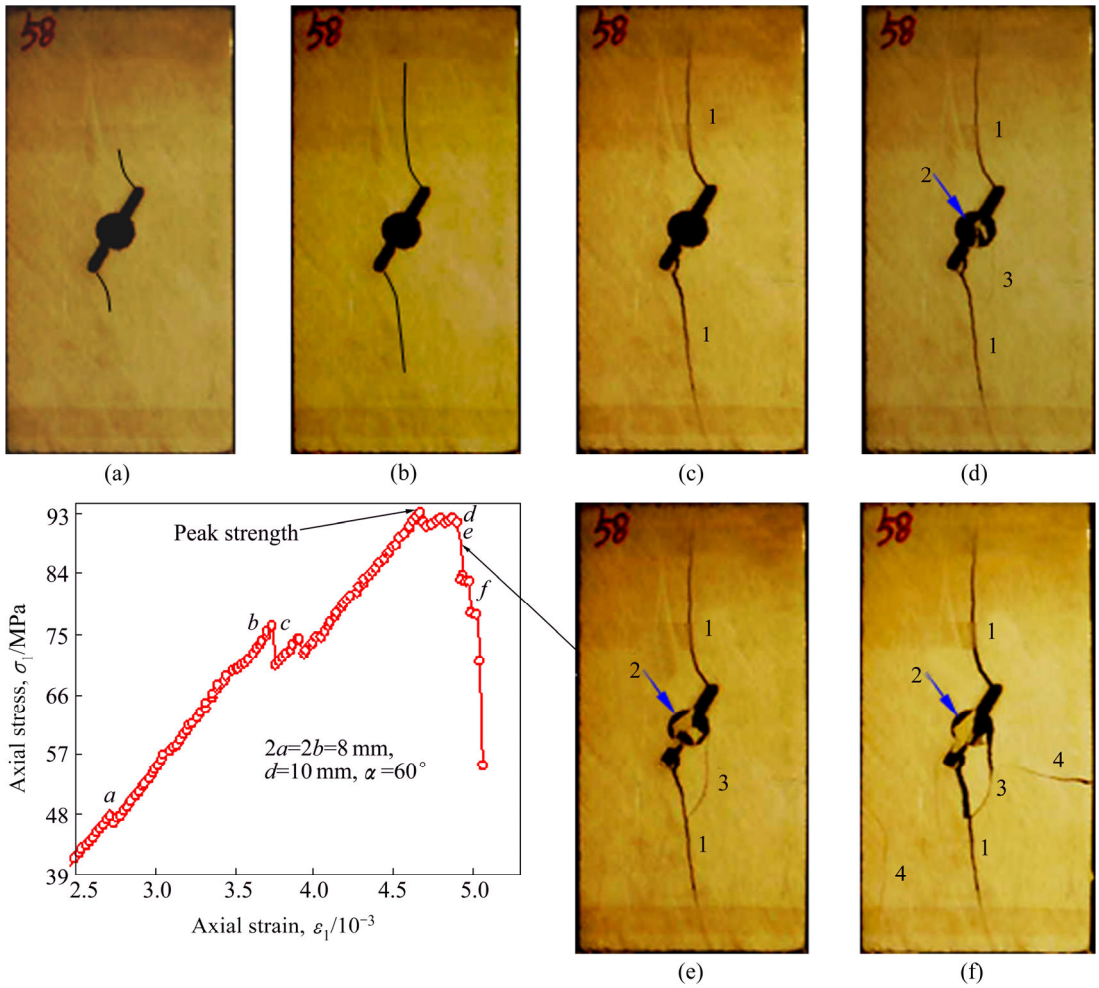

Fig. 15 Relation between local axial stress−axial strain curve and real-time crack coalescence of brittle sandstone specimen containing combined flaws (d=10 mm, $2a$=$2b$=8 mm, α=60°) under uniaxial compression: (a) σ_1=47.86→46.77 MPa; (b) σ_1= 75.33 MPa; (c) σ_1=76.05→70.39 MPa; (d) σ_1=92.04→91.42 MPa; (e) σ_1=91.61→83.62 MPa; (f) σ_1=82.62→78.17 MPa

we do not analyze in detail the effect of real-time crack coalescence process on the strength and deformation behavior any more due to similar influence with Fig. 14. However, it needs to be noted that the specimen begins to initiate the first crack 1 when the axial stress is loaded to point *a* (σ_1=47.86 MPa=51.5% σ_c). But the first crack does not propagate rapidly the specimen boundary, which is different from that shown in Fig. 14. From points *b* to *c* in Fig. 15, the first crack 1 in the specimen evolves rapidly to the specimen boundary; moreover, the crack width increases obviously. Afterwards, as axial deformation increases, the axial stress reaches the point *d*, at this time, the cracks 2 and 3 appear simultaneously, but the crack 3 is obscure. The continuous increase of axial deformation leads to gradual coalescence of hole collapse (crack 2) despite gradual drop of axial stress, moreover, the width of crack 3 increases step by step.

6 Conclusions

1) Tested intact sandstone specimen is a kind of typical brittle rock and takes on typically axial splitting failure. Compared with the intact specimen, the mechanical parameters of sandstone specimens containing combined flaws in uniaxial compression are all lower. The uniaxial compressive strength and elastic moduli have the same tendency with the increase of fissure angle, i.e., firstly increase and then decrease, finally increase with increased fissure angle. The heterogeneity has no nearly any influence on the strength and deformation parameters of brittle sandstone specimens containing combined flaws, but changing the complete axial stress−axial strain curve including brittleness and ductility after peak strength.

2) Based on their geometry and crack propagation mechanism (tensile, hole collapse, far-field crack and surface spalling) for combined flaws in response to the applied axial loads, nine different crack types are identified. The results indicate that the failure mode of sandstone specimens containing combined flaws is all a mixture of several cracks among nine crack types. The tensile crack V is the first crack to initiate, and is only observed in two specimens with α=15°, which shows that this fissure angle makes the specimen containing combined flaws (*d*=10 mm, 2*a*=2*b*=8 mm) easier to emanate this tensile crack V from hole-edge along the direction of axial stress. However, the tensile crack I is usually the first crack initiated from the tips of pre-existing fissures for flawed specimens with the fissure angle α>15°. During the whole loading, the AE counts of brittle sandstone specimens containing combined flaws under uniaxial compression are recorded simultaneously to analyze the influence of different loading stages and fissure angle on the AE behaviors.

3) The photographic monitoring is also adopted during uniaxial compression test to confirm the sequence of crack coalescence in brittle sandstone specimens containing combined flaws. Based on the photographic monitoring results, the real-time crack coalescence process of sandstone containing combined flaws are identified and characterized. Moreover, the corresponding axial stress of crack coalescence in brittle sandstone specimens containing combined flaws is also obtained. Each larger stress drop in axial strain−axial strain curve indicates a larger crack coalescence. According to recorded monitoring results, the effect of crack coalescence process on the strength and deformation behavior is analyzed in detail for brittle sandstone specimens containing combined flaws.

References

[1] NEMAT-NASSER S, HORII H. Compression-induced nonlinear crack extension with application to splitting, exfoliation, and rockburst [J]. Journal of Geophysical Research, 1982, 87(B8): 6805−6821.

[2] WONG R H C, CHAU K T. Crack coalescence in a rock-like material containing two cracks [J]. International Journal of Rock Mechanics and Mining Sciences, 1998, 35: 147−164.

[3] PRUDENCIO M, VAN SINT JAN M. Strength and failure modes of rock mass models with non-persistent joints [J]. International Journal of Rock Mechanics and Mining Sciences, 2007, 44(6): 890−902.

[4] PARK C H, BOBET A. Crack coalescence in specimens with open and closed flaws: A comparison [J]. International Journal of Rock Mechanics and Mining Sciences, 2009, 46(5): 819−829.

[5] FENG X T, DING W X, ZHANG D X. Multi-crack interaction in limestone subject to stress and flow of chemical solutions [J]. International Journal of Rock Mechanics and Mining Sciences, 2009, 46(1): 159−171

[6] WONG L N Y, EINSTEIN H H. Systematic evaluation of cracking behavior in specimens containing single flaws under uniaxial compression [J]. International Journal of Rock Mechanics and Mining Sciences, 2009, 46(2): 239−249.

[7] YANG S Q, DAI Y H, HAN L J, JIN Z Q. Experimental study on mechanical behavior of brittle marble specimens containing different flaws under uniaxial compression [J]. Engineering Fracture Mechanics, 2009, 76(12): 1833−1845.

[8] YANG S Q, JIANG Y Z, XU W Y, CHEN X Q. Experimental investigation on strength and failure behavior of pre-cracked marble under conventional triaxial compression [J]. International Journal of Solids and Structures, 2008, 45(17): 4796−4819.

[9] FUJII Y, ISHIJIMA Y. Consideration of fracture growth from an inclined slit and inclined initial fracture at the surface of rock and mortar in compression [J]. International Journal of Rock Mechanics and Mining Sciences, 2004, 41: 1035−1041.

[10] LU Zu-de, DING Wu-xiu, FENG Xia-ting, ZHANG You-liang. Experimental study on mechanical-hydraulic-chemical coupling process in cracked rocks [J]. Chinese Journal of Rock Mechanics and Engineering, 2008, 27(4): 796−804. (in Chinese)

[11] YANG S Q, JING H W. Strength failure and crack coalescence behavior of brittle sandstone specimens containing a single fissure

under uniaxial compression [J]. International Journal of Fracture, 2011, 68(2): 227−250.

[12] LI Y P, CHEN L Z, WANG Y H. Experimental research on pre-cracked marble under compression [J]. International Journal of Solids and Structures, 2005, 42: 2505−2516.

[13] LABUZ J F, CATTANEO S, CHEN L H. Acoustic emission at failure in quasi-brittle materials [J]. Construction and Building Materials, 2001, 15: 225−233.

[14] CHANG S H, LEE C I. Estimation of cracking and damage mechanisms in rock under triaxial compression by moment tensor analysis of acoustic emission [J]. International Journal of Rock Mechanics and Mining Sciences, 2004, 41: 1069−1086.

[15] PESTMAN B J, VAN MUNSTER J G. An acoustic emission study of damage development and stress-memory effects in sandstone [J]. International Journal of Rock Mechanics and Mining Sciences & Geomechanics Abstracts, 1996, 33(6): 585−593.

[16] LI Y H, ZHU H H, JING H W. Experimental observation of shear deformation patterns in sands using digital photogrammetry [J]. Geotechnical Special Publication (ASCE), 2006, 149(6): 120−127.

[17] SHAH S G, CHANDRA KISHEN J M. Fracture properties of concrete-concrete interfaces using digital image correlation [J]. Experimental Mechanics, 2011, 51: 303−313.

[18] LI Yuan-hai, JING Hong-wen, LIU Gang, ZHOU Zhi-guo. Study on application of digital close range photogrammetry to model test of tunnel in jointed rock masses [J]. Chinese Journal of Rock Mechanics and Engineering, 2007, 26(8): 1684−1690. (in Chinese)

[19] LI Yuan-hai, JING Hong-wen, ZHU He-hua, UENO K. A technique of identifying the shear band accurately in granular soil using image correlation analysis [J]. Rock and Soil Mechanics, 2007, 28(3): 522−526. (in Chinese)

(Edited by HE Yun-bin)